In Vivo Evaluation of ^{18}F-MNI698: An ^{18}F-Labeled Radiotracer for Imaging of Serotonin 4 Receptors in Brain

Adriana Alexandre S. Tavares[1], Fabien Caillé[1,2], Olivier Barret[1,2], Caroline Papin[1,2], Hsiaoju Lee[1,2], Thomas J. Morley[1,2], Krista Fowles[3], Daniel Holden[3], John P. Seibyl[1–3], David Alagille[1,2], and Gilles D. Tamagnan[1,2]

[1]Molecular NeuroImaging, LLC, New Haven, Connecticut; [2]Institute for Neurodegenerative Disorders, New Haven, Connecticut; and [3]Yale University, New Haven, Connecticut

Serotonin 4 receptors (5-hydroxytryptamine receptor 4 [5HT4R]) hold promise as a novel therapeutic approach to multiple brain disorders, including Alzheimer and Huntington disease. In vivo imaging of these receptors with selective 5HT4R radiotracers and PET would be valuable to investigate alterations in 5HT4R in different brain disorders and to assist drug discovery. In this study, ^{18}F-MNI698 was evaluated as a potential PET radiotracer for imaging of 5HT4R in the brain. **Methods:** Eighteen PET studies were performed in 3 adult rhesus monkeys. The radiotracer was administered as a bolus intravenous injection or bolus plus constant infusion (time that would be required to inject the bolus at the infusion rate = 60 min), and arterial blood was collected for data quantification. Kinetic models were used to estimate distribution volumes and binding potentials, for which the cerebellum was used as a reference region. ^{18}F-MNI698 test–retest variability and upper mass dose limits were determined. Preblocking studies using several doses of SB204070, a selective 5HT4R antagonist, were performed. **Results:** ^{18}F-MNI698 avidly entered the monkey brain (peak percentage injected dose of ~6.6%), and its brain distribution was consistent with known 5HT4R densities. At 120 min after bolus injection and after the start of radiotracer infusion, only less than 5% and approximately 10% parent compound was present in blood, respectively. Measured binding potentials were underestimated by 22%–36% when noninvasive methods were used for data quantification in comparison with invasive methods. A good agreement was found between test–retest measurements. The radiotracer upper mass dose limit (<5% occupancy) was determined to be 13.1 μg per 70 kg of body weight. SB204070 blocked the radiotracer binding in a dose-dependent manner. **Conclusion:** Data indicate that ^{18}F-MNI698 is a promising PET radiotracer for imaging of 5HT4R in the brain, and human studies are warranted based on these study results.

Key Words: 5HT4R; ^{18}F-MNI698; test–retest; mass effect; SB204070

J Nucl Med 2014; 55:858–864
DOI: 10.2967/jnumed.113.132712

The serotonin 4 receptors (5-hydroxytryptamine receptor 4 [5HT4R]) are well-characterized G-protein–coupled receptors that can be found in a variety of organs and tissues, including the brain (*1–3*). High densities of 5HT4R are detected in the basal ganglia and limbic structures in the brain, whereas low densities are measured in the neocortex and negligible levels of binding are found in the cerebellum (*4–7*). The 5HT4Rs are involved in different brain functions and dysregulation of these receptors has been implicated in depression (*8–10*), attention-deficit/hyperactivity disorder (*11,12*), anorexia and obesity (*12,13*). Furthermore, autoradiographic examinations of brain tissue from Alzheimer disease subjects have shown a marked loss of 5HT4R in hippocampal and cortical regions, which is consistent with a role of 5HT4R in cognition; and brain tissue from Huntington disease subjects demonstrated a reduction of 5HT4R in the putamen (*7*). Evidence that 5HT4R agonists mediate enhancement of cognitive function in vivo and amyloid precursor protein processing in vitro has also been published recently (*14*). In a mouse model of Alzheimer disease, chronic administration of a 5HT4R agonist decreased soluble and insoluble β-amyloid plaques in the hippocampus (*15*).

A selective 5HT4R radiotracer would allow for in vivo imaging studies examining disease progression and treatment response in different brain disorders. In addition, it would also be valuable in studies assessing drugs targeting the 5HT4R, thus supporting drug discovery. The most promising 5HT4R radiotracers developed so far are the ^{11}C-labeled SB207145 and the ^{123}I-labeled SB207710 (*16–19*). The latter displayed high affinity for 5HT4R and was subsequently evaluated in nonhuman primates (*19*). The former has been evaluated in both animal studies and human studies (*16–18*). Although imaging data obtained using ^{11}C-SB207145 demonstrated its suitability for imaging 5HT4R in the brain, a radiotracer incorporating the longer-lived ^{18}F is desirable. An ^{18}F-labeled radiotracer has the advantage of providing images with higher resolution and sensitivity than those obtained with an ^{123}I-labeled radiotracer, without the need for a cyclotron in the imaging facility as required for a ^{11}C-labeled radiotracer. Recently, we reported the synthesis of novel ^{18}F-labeled radiotracers for imaging of 5HT4R in the brain, identifying ^{18}F-MNI698 as the lead radiotracer (*20*). The current study aimed to characterize the in vivo pharmacokinetics of ^{18}F-MNI698 in the nonhuman primate brain, to determine test–retest variability, to assess the radiotracer upper mass dose limit to avoid mass dose effects, and to measure receptor occupancy with a selective 5HT4R antagonist drug, SB204070.

MATERIALS AND METHODS

Radiotracer and Drug Preparation

^{18}F-MNI698 was prepared as described previously (*20*), with an average decay-corrected radiochemical yield of approximately 3% (reaction time of 80 min; $n = 14$), a radiochemical purity greater than 97%, and a specific activity at the end of the synthesis between 45 and

Received Oct. 7, 2013; revision accepted Jan. 27, 2014.
For correspondence or reprints contact: Adriana Alexandre S. Tavares, Molecular NeuroImaging, 60 Temple St., Suite 8B, New Haven, CT 06510.
E-mail: adriana_tavares@msn.com
Published online Mar. 31, 2014.

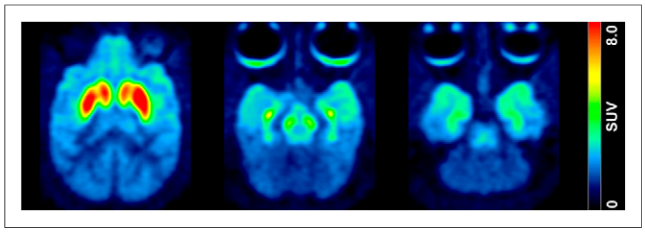

FIGURE 1. Representative PET SUV sum images (0–120 min) of ^{18}F-MNI698 distribution in monkey brain. High uptake is observed in target regions: caudate and putamen (left), substantia nigra (middle), and hippocampal formation (right).

1,090 GBq/μmol (1.2–29.4 Ci/μmol). For the mass dose experiments, different amounts of cold MNI698 were added to the radiotracer solution.

SB204070 was purchased from Tocris and formulated in 100 mM (pH 5.5) acetate buffer. All solutions were filtered through a 0.2-μm filter into a sterile empty vial and were tested for sterility and pyrogen content.

Animals

All experiments were conducted in accordance with institutional animal care protocols in compliance with federal regulations. Three adult rhesus monkeys, 1 male and 2 females (*Macaca mulatta*; mean weight ± SD, 7.00 ± 1.02 kg), were used for this study. Details on animal preparation and monitoring can be found in the supplemental file (supplemental materials are available at http://jnm.snmjournals.org).

PET Studies

Study Design. Eighteen PET scans were obtained with ^{18}F-MNI698 (mean injected radioactivity ± SD, 135.42 ± 41.37 MBq). Scans were acquired after intravenous bolus injection or bolus plus constant infusion (B+CI; time that would be required to inject the bolus at the infusion rate [K_{bol}] = 60 min) of ^{18}F-MNI698. Test–retest scans were obtained in 2 rhesus monkeys after intravenous B+CI of the radiotracer, with 2- to 4-wk intervals between test and retest imaging sessions. Rhesus monkey 1 was scanned 4 times at baseline conditions, and rhesus monkey 2 was scanned twice under baseline conditions. Studies aiming to assess the radiotracer mass dose effects on receptor occupancy and those estimating MNI698 dose resulting in 50% receptor occupancy (ID_{50}) in vivo were acquired after intravenous B+CI of a radiotracer solution containing high levels of mass doses. In a separate set of studies, preblocking experiments with a selective 5HT4R antagonist drug, SB204070, were performed after intravenous B+CI of the radiotracer. Rhesus monkey 1 was scanned after preblocking with SB204070 at 4 different doses (0.3, 5.0, 50.0, and 500.0 μg/kg), and rhesus monkey 2 was scanned after preblocking with SB204070 at 3 different doses (0.6, 10.0, and 150.0 μg/kg). SB204070 was given as a 10-min intravenous injection at approximately 30 min before radiotracer administration.

Image Acquisition and Reconstruction. All PET data were acquired using a microPET Focus220 scanner (Siemens). A transmission scan was acquired, and then, immediately after radiotracer administration, a 120-min emission scan was obtained using 3-dimentional mode as follows: 6 × 30 s, 3 × 60 s, 2 × 2 min, and 22 × 5 min. The dynamic PET sinograms were corrected for randoms, dead time, scatter, and attenuation. Subsequently, acquired frames were reconstructed using filtered backprojection with a Shepp–Logan filter and image size of 256 × 256.

Blood Analysis. Arterial blood samples were collected each 45 s until 6 min after injection and then at 8, 10, 15, 20, 25, 30, 45, 60, 90, and 120 min. With the exception of the samples collected for metabolite analysis (3.5 mL each), all blood samples were 1 mL each. Samples for metabolite analysis were collected at 6, 15, 30, 60, and 120 min after radiotracer bolus injection or at 3, 6, 10, 15, 30, 60, and 120 min after radiotracer B+CI. The potent esterase inhibitor dichlorvos was added to all blood sampling tubes (200 μg/mL of blood) to inhibit metabolism of the parent compound in vitro. The need for a protease inhibitor is consistent with previous observations indicating that for this family of compounds, accurate metabolite quantification requires the addition of protease inhibitors to each blood sample (*16–18*). After blood collection, all samples were kept on ice until analyzed. Details on blood sample processing and analysis are provided in the supplemental materials.

Image Processing. Reconstructed scans were imported into PMOD 3.405 software (PMOD Technologies). An in-house–developed rhesus monkey brain MR imaging template was used for image coregistration and placement of volumes of interest for quantification of radiotracer uptake. Each monkey underwent T1-weighted MR imaging with a Siemens Trio System (Siemens) at 3T (repetition time, 2.0 s; echo time, 2.74 ms; inversion time, 1.11 s; and flip angle, 7°). Acquired images were reduced from an initial matrix of 256 × 256 with 176 axial slices (axial slice thickness, 0.6 mm) to a 128 × 128 matrix with 120 axial slices (axial slice thickness, 1.2 mm). The following brain regions were manually drawn on the MR image: striatum, caudate, putamen, hippocampus, substantia nigra, globus pallidus, thalamus, frontal cortex, occipital cortex, parietal cortex, temporal cortex, and cerebellum. Average images of ^{18}F-MNI698 PET data were generated by averaging the scans with highest brain uptake. Then, the average image was coregistered to the rhesus MR imaging template. The transformation matrix was saved and subsequently applied to the dynamic PET series. Finally, MR imaging–derived volumes of interest were applied to the coregistered PET images for image quantification.

Data Analysis. Time–activity curves were generated and standardized uptake values (SUVs) calculated as concentration in the volume of interest divided by injected dose divided by animal weight. The SUVs in target regions were divided by SUVs determined in the cerebellum, the brain region with the lowest concentration of 5HT4R (*4–7*), to generate SUV ratios (SUVrs).

Kinetic modeling was performed using compartmental analysis (1-tissue [1T] and 2-tissue [2T] models) and Logan graphical analysis to estimate the volume of distribution (V_T) in different brain regions (*21,22*). The 1T and 2T model-fitting performance was evaluated using the Akaike information criterion (AIC) and the model selection criterion (MSC), where the preferred model had the lowest AIC and highest MSC. The selected

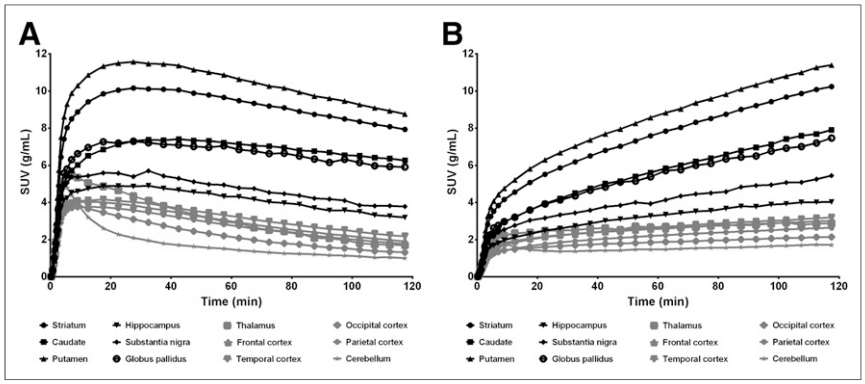

FIGURE 2. Representative SUV time–activity curves in different brain regions after bolus (A) or B+CI (B) injection of radiotracer.

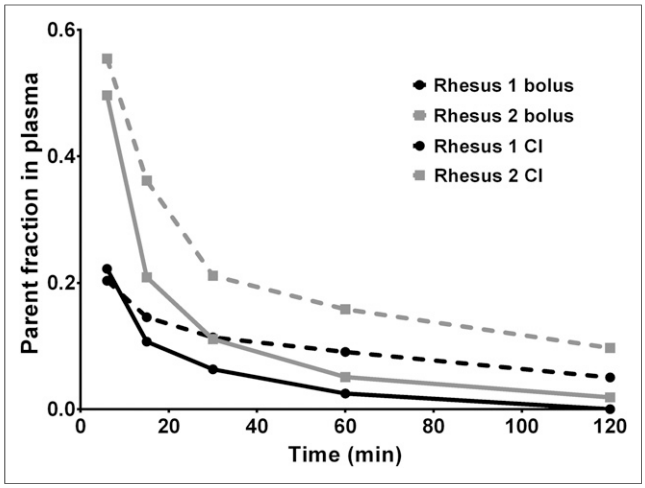

FIGURE 3. Parent fraction profile in plasma over time after bolus (full lines) or B+CI (dashed lines) injection of ^{18}F-MNI698. CI = constant infusion.

identifiability criterion was the percentage SE (%SE) of V_T estimates. The binding potential BP_{ND}, defined at equilibrium as the ratio of specifically bound to nondisplaceable radiotracer uptake in tissue (*21*), was calculated indirectly as $(V_T - V_{ND})/V_{ND}$, where V_{ND} was the V_T of the reference region. In addition, BP_{ND}s were also estimated using noninvasive kinetic models—namely, the simplified reference tissue model (SRTM) and the Logan noninvasive graphical analysis (*23,24*)—as well as from the SUVrs at pseudoequilibrium (60–90 min after radiotracer injection) as BP_{ND} = SUVr-1. The cerebellum was used as a reference region for all BP_{ND} estimations.

Test–retest variability was calculated as the absolute of the SD of all measurements divided by the average value, expressed as a percentage.

For the mass effect study, all mass doses (D) were normalized to 70 kg of body weight to facilitate comparison between animals and to predict the mass dose limits for an adult human. The methodology used to estimate the radiotracer ID_{50} and to calculate the upper mass dose limits that will result in 5% or 10% receptor occupancy (D_5 or D_{10}, respectively) was based on previously published literature (supplemental materials) (*25*).

The 5HT4R occupancy induced by administration of SB204070 was calculated using 2 methods: percentage change of BP_{ND} between baseline and SB204070 blocking experiments (Eq. 1) and the Lassen plot method (Eq. 2) (*26*).

$$\text{Occupancy} = \frac{BP_{ND}\text{baseline} - BP_{ND}\text{preblocking}}{BP_{ND}\text{baseline}} \qquad \text{Eq. 1}$$

$$O = \frac{V_T\text{baseline} - V_T\text{preblocking}}{V_T\text{baseline} - V_{ND}}, \qquad \text{Eq. 2}$$

which, when represented graphically for several regions ($x = V_T$ baseline, $y = V_T$ baseline – V_T preblocking), produces a linear relationship, where the x intercept equals V_{ND} and the gradient equals global occupancy (O). Individual brain regions occupancy was also determined by deriving V_{ND} from the Lassen plot and subsequently applying Eq. 2 for occupancy quantification.

The occupancies measured with different methods were subsequently corrected for potential mass dose effects—that is, self-occupancy (supplemental materials).

RESULTS

In vivo PET studies in rhesus monkeys showed that, after intravenous bolus injection, ^{18}F-MNI698 rapidly entered the brain,

TABLE 1
^{18}F-MNI698 Kinetic Modeling Results Obtained Using 2T, 1T, and Logan Graphical Analysis with Arterial Input Function

Brain region	2T model				1T model				Logan arterial	
	V_T	%SE	AIC	MSC	V_T	%SE	AIC	MSC	V_T	%SE
Caudate	210.15 ± 44.55	2.74 ± 1.03	−79.91 ± 27.04	6.94 ± 0.70	213.55 ± 38.32	2.65 ± 0.59	−69.75 ± 15.16	6.60 ± 0.50	185.93 ± 32.99	2.04 ± 0.54
Putamen	224.26 ± 66.30	1.27 ± 0.37	−95.82 ± 13.63	7.33 ± 0.36	223.32 ± 62.88	1.39 ± 0.32	−76.95 ± 16.15	6.71 ± 0.68	206.83 ± 58.56	1.08 ± 0.39
Striatum	214.81 ± 56.50	1.40 ± 0.41	−98.07 ± 17.78	7.42 ± 0.40	215.44 ± 52.52	1.55 ± 0.35	−79.57 ± 16.64	6.82 ± 0.64	197.17 ± 48.66	1.15 ± 0.38
Globus pallidus	166.18 ± 46.58	3.12 ± 0.62	−59.71 ± 11.97	6.30 ± 0.41	168.58 ± 39.87	2.91 ± 0.53	−50.31 ± 15.62	6.01 ± 0.61	150.60 ± 38.67	3.05 ± 0.67
Substantia nigra	96.05 ± 19.46	5.31 ± 5.08	−34.71 ± 20.54	5.40 ± 0.73	91.85 ± 15.66	2.96 ± 0.75	−14.71 ± 20.75	4.83 ± 0.70	88.36 ± 18.22	2.97 ± 0.88
Hippocampus	68.13 ± 16.23	1.61 ± 0.32	−59.51 ± 19.69	6.10 ± 0.72	67.32 ± 14.76	1.76 ± 0.37	−33.57 ± 27.67	5.33 ± 0.90	64.21 ± 14.95	1.45 ± 0.17
Occipital cortex	35.90 ± 3.66	2.63 ± 3.63	−78.54 ± 30.34	6.36 ± 0.93	32.73 ± 2.58	1.63 ± 0.37	2.06 ± 24.78	3.96 ± 0.79	32.90 ± 1.93	1.01 ± 0.43
Cerebellum	27.12 ± 4.00	3.74 ± 1.47	−44.45 ± 26.01	4.98 ± 0.78	19.05 ± 3.72	4.44 ± 0.32	97.87 ± 23.45	0.85 ± 0.33	23.16 ± 5.10	1.82 ± 0.38

Data are mean ± SD (n = 6).

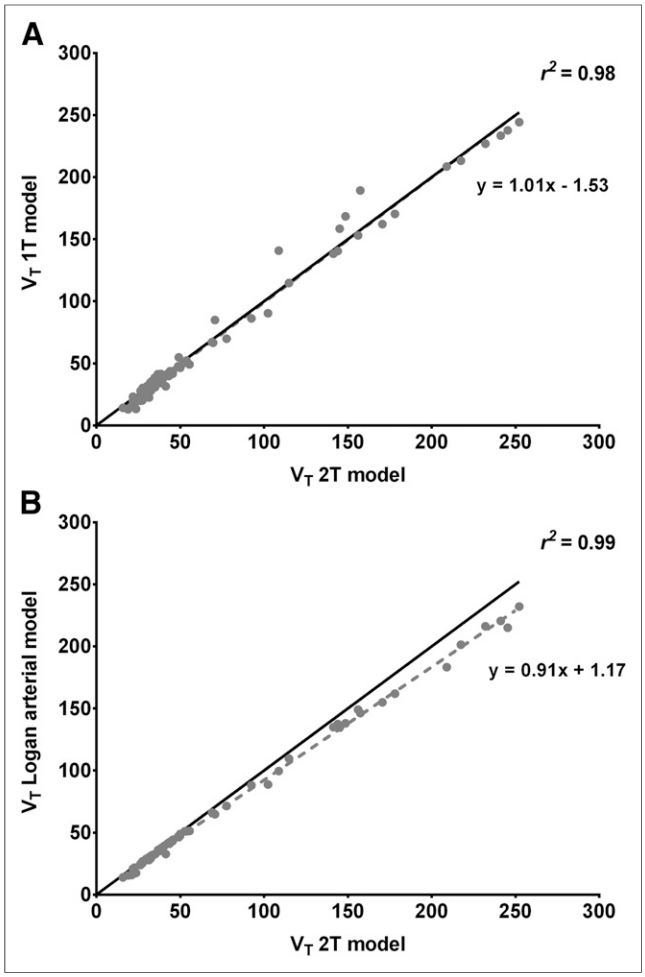

FIGURE 4. Comparative analysis between V_Ts obtained using 2T model and 1T model (A) or Logan graphical analysis (B) ($r^2 > 0.90$ for both graphs). Correlations are close to line of identity (shown as dark bold line).

with a peak percentage injected dose (%ID) in the whole brain of 6.6% ± 0.5% ($n = 3$). ^{18}F-MNI698 distribution was consistent with known 5HT4R densities, being highest in the basal ganglia and limbic structures and lowest in the cerebellum (Figs. 1 and 2A). After intravenous bolus injection, a rapid in vivo metabolism of the radiotracer in blood was observed (Fig. 3) and at 2 h after injection less than 5% of parent was detected in plasma, which was within or below the instrumentation detection limits. When ^{18}F-MNI698 was injected as a B+CI, the parent fraction in plasma at 2 h after injection improved to approximately 10% (Fig. 3). Regional time–activity curves in the brain after intravenous B+CI of ^{18}F-MNI698 are shown in Figure 2B.

Within the invasive compartmental methods of analysis, the 2T was found to be the preferred model, compared with 1T (lowest AIC and highest MSC values were obtained with the 2T model) (Table 1). The high-uptake-region time–activity curves were adequately fitted by both compartmental methods, but the 1T fitting was biased in the low-uptake regions (Supplemental Fig. 1). The Logan graphical analysis (t* = 25 min) was also able to fit the data adequately (Supplemental Fig. 1), and overall it was able to estimate V_Ts with the lowest %SE of all investigated invasive models (Table 1). The V_Ts determined by the 2T model were comparable to those estimated using the 1T model (Fig. 4A) and approximately 9.0% higher than the V_Ts estimated by the Logan graphical analysis, especially in the high-uptake regions (Fig. 4B; Table 1).

Apart from the BP_{ND}s determined using the 1T model, all BP_{ND}s measured in target regions ranged between 1.5 in the hippocampus and 7.8 in the putamen when invasive methods of quantification were used and between 1.3 in the hippocampus and 6.1 in the putamen when noninvasive methods of analysis were used (Table 2). The use of noninvasive methods of quantification, compared with the invasive methods, resulted in an underestimation of the BP_{ND}s, which was more pronounced in the brain regions with high density of 5HT4R (Table 2; Supplemental Fig. 2). This underestimation was between 22% and 36% depending on the method of analysis used. The Logan noninvasive graphical analysis (t* = 25 min) was the noninvasive method of quantification with the least underestimation of BP_{ND}s in comparison with invasive modeling (Fig. 5).

Test–retest V_Ts estimated in target regions showed an agreement between measurements, where the percentage variability was 13% or less. The variability of BP_{ND}s for test–retest measurements was overall lower for noninvasive methods of quantification than for invasive methods and was on average 15% or less (Table 3).

Increasing the mass dose reduced the BP_{ND}s for both studies ($\alpha < 1$). The radiotracer ID_{50} was estimated to be 248.3 ± 56.6 μg for a 70-kg body weight (i.e., ~3.5 μg/kg) (Table 4). The quantification of striatal 5HT4R occupancy by SB204070 using different methods is shown in Figure 6. A dose-dependent receptor occupancy was observed and doses of SB204070 of 50 μg/kg or more induced greater than 90% occupancy. The relationship between receptor occupancy measured with invasive methods versus noninvasive methods was linear, correlated strongly, and was close

TABLE 2
BP_{ND}s Estimated Using Different Quantification Methods

Brain region	BP_{ND} 2T	BP_{ND} 1T	BP_{ND} Logan arterial	BP_{ND} Logan reference	BP_{ND} SRTM	BP_{ND} SUVr
Caudate	6.73 ± 1.05	10.29 ± 1.07	7.15 ± 0.92	4.60 ± 0.94	4.53 ± 0.91	3.88 ± 0.75
Putamen	7.15 ± 1.61	10.59 ± 1.57	7.85 ± 1.03	6.13 ± 0.31	6.07 ± 0.31	5.41 ± 0.20
Striatum	6.84 ± 1.32	10.26 ± 1.20	7.50 ± 0.81	5.58 ± 0.42	3.68 ± 0.25	4.88 ± 0.27
Globus pallidus	5.04 ± 1.01	7.85 ± 1.06	5.48 ± 0.63	3.73 ± 0.25	1.51 ± 0.22	3.19 ± 0.14
Substantia nigra	2.52 ± 0.32	3.88 ± 0.58	2.85 ± 0.41	2.24 ± 0.33	5.51 ± 0.41	2.01 ± 0.20
Hippocampus	1.49 ± 0.34	2.54 ± 0.36	1.78 ± 0.27	1.52 ± 0.22	2.22 ± 0.34	1.33 ± 0.17
Occipital cortex	0.34 ± 0.13	0.78 ± 0.41	0.48 ± 0.33	0.52 ± 0.38	0.54 ± 0.39	0.44 ± 0.32

Data are mean ± SD ($n = 6$).

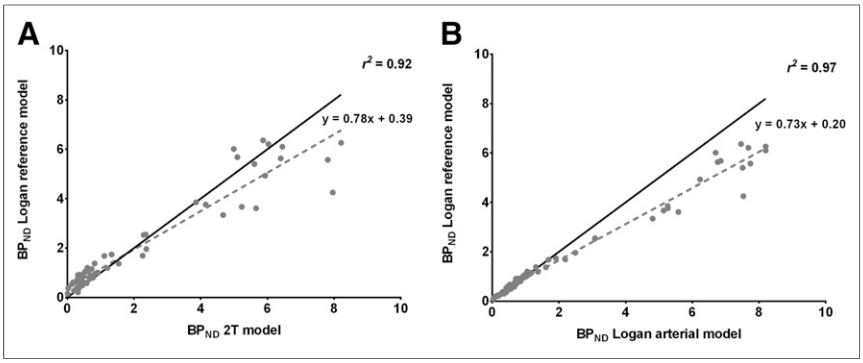

FIGURE 5. Comparative analysis between BP_{ND}s obtained using 2T model and Logan noninvasive reference model (A), and between Logan graphical analysis using arterial input function and Logan noninvasive reference model (B) ($r^2 > 0.90$). Line of identity is shown as dark bold line.

to the line of identity (Supplemental Figs. 3A and 3B). The V_Ts measured in the reference region (i.e., the cerebellum) at baseline were not statistically significantly different from those measured at preblocking conditions with high doses of SB204070 ($P > 0.05$, 2 tailed t test) and were similar to derived V_{ND}s from the Lassen plots (Supplemental Fig. 3C).

DISCUSSION

The present study investigated a new ^{18}F-labeled radiotracer for imaging 5HT4R in the brain in nonhuman primates. To our knowledge, ^{18}F-MNI698 is the first successful ^{18}F-labeled radiotracer for imaging 5HT4R in the nonhuman primate brain developed to date. After intravenous bolus injection, ^{18}F-MNI698 displayed high brain penetration, with a peak %ID in the whole brain of 6.6% and peak SUVs as high as 8.0 in target regions. In addition, the radioactivity distribution in the brain was consistent with known 5HT4R densities and agreed with the reported brain labeling of ^{11}C-SB207145, the only other known PET radiotracer for imaging of 5HT4R in the brain (*4–7,16–18*). The good brain penetration of ^{18}F-MNI698 compares favorably with other radiotracers previously developed. For example, intravenous injection of ^{123}I-SB207711 into cynomolgus monkeys yielded a peak %ID in the whole brain of approximately 2.28% (*19*).

After intravenous bolus injection, ^{18}F-MNI698 was rapidly metabolized in vivo in rhesus monkey blood. Previous studies with another 5HT4R radiotracer structurally similar to ^{18}F-MNI698 have found similar results in different species (*16,18*). To improve the reliability of metabolite quantification, ^{18}F-MNI698 was injected as a B+CI and data subsequently quantified using this imaging paradigm. This procedure improved blood and metabolite quantification, allowing for adequate kinetic modeling analysis using more robust arterial input functions.

The pharmacokinetics of the radiotracer were reversible and well described by both the 2T model and the invasive Logan graphical analysis. High BP_{ND}s of approximately 1.3–7.0 were measured in target regions using either invasive or noninvasive methods of analysis. Previous studies using Göttingen minipigs and ^{11}C-SB207145, a potent radiotracer for imaging 5HT4R in the brain, reported BP_{ND}s in the striatum of around 2.0 (*17*). In humans, ^{11}C-SB207145 BP_{ND}s in the striatum and hippocampus were determined to be around 2.6–4.2 and 0.8–1.1, respectively (*18,27*). ^{123}I-SB207711 BP_{ND}s in rodents and cynomolgus monkeys were found to be approximately 2.4 and 3.0, respectively (*19*). Although it is not possible to directly compare our data in nonhuman primates with rodent, minipig, or human data previously published, due to species and acquisition mode differences, the BP_{ND}s of ^{18}F-MNI698 in target regions compare favorably with other 5HT4R radiotracers previously reported. The high BP_{ND}s measured with ^{18}F-MNI698 would provide the opportunity to assess 5HT4R in areas with moderate to high densities (e.g., substantia nigra and hippocampus), which would be potentially more challenging to interrogate with radiotracers with lower BP_{ND}s.

Noninvasive quantification methods were able to estimate BP_{ND}s, although a negative bias of 22%–36% was obtained with those methods, especially in the slowest kinetic target regions. A similar observation has been reported for ^{11}C-SB207145 in humans (*18*). The underestimation of BP_{ND}s observed with the SRTM compared with invasive methods is likely due to violations

TABLE 3
Test–Retest Results in Target Regions for Each Individual Rhesus Monkey

Rhesus monkey identification no.	Kinetic model	Percentage variability in different brain regions					
		Caudate	Putamen	Striatum	Globus pallidus	Substantia nigra	Hippocampus
1	V_T 2T	8.97	10.37	9.97	13.19	11.20	12.24
	V_T Logan arterial	9.07	9.33	8.95	10.87	11.83	11.19
	BP_{ND} 2T	15.69	13.81	14.10	14.21	13.75	20.61
	BP_{ND} Logan arterial	13.34	12.71	12.55	14.15	17.41	19.36
	BP_{ND} Logan reference	7.43	5.94	6.39	8.48	14.77	14.16
	BP_{ND} SRTM	8.04	6.06	6.73	8.62	15.55	14.13
	BP_{ND} SUVr	5.59	4.33	4.57	5.33	9.71	12.64
2	V_T 2T	0.61	1.84	2.25	3.87	6.58	0.97
	V_T Logan arterial	1.31	0.23	0.28	6.78	6.88	1.40
	BP_{ND} 2T	9.85	11.46	11.82	5.12	1.83	12.75
	BP_{ND} Logan arterial	6.23	7.55	8.10	0.04	0.05	8.48
	BP_{ND} Logan reference	8.61	4.00	6.30	1.67	0.56	2.48
	BP_{ND} SRTM	8.69	3.69	6.16	1.53	1.12	2.47
	BP_{ND} SUVr	5.11	0.11	2.12	5.09	1.76	0.17

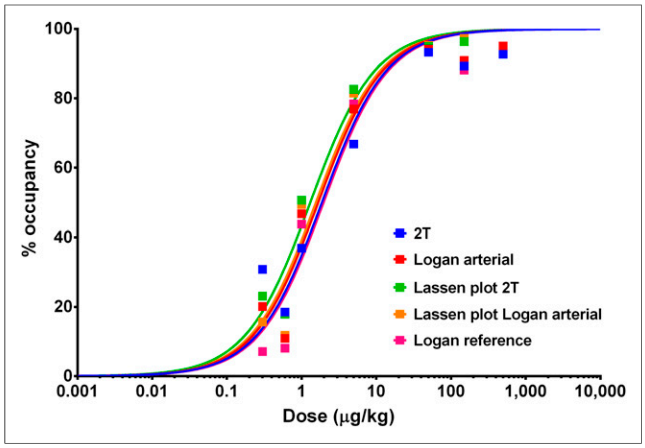

FIGURE 6. SB204070 dose-dependent occupancy curve measured using PET with ^{18}F-MNI698 in striatum of rhesus monkeys (drug dose resulting in 50% receptor occupancy was 1.87, 1.67, 1.31, 1.55, and 1.97 μg/kg using 2T, Logan plot, 2T with V_{ND} derived from Lassen plot, Logan plot with V_{ND} derived from Lassen plot, and noninvasive Logan plot, respectively).

of SRTM assumptions that require 1T in the reference region (*23*). Interestingly, the BP_{ND} underestimation determined when using the noninvasive methods for data quantification was still present even when applying the Logan noncompartmental analysis, although this bias was marginally smaller than the bias measured for the SRTM. It is unlikely this underestimation is due to specific binding in the reference region (i.e., the cerebellum), given that previous studies have shown negligible levels of 5HT4R in the cerebellum (*4–7*). Furthermore, in this study, the cerebellum had the lowest uptake and V_Ts of all investigated regions, and preblocking studies with SB204070 showed no significant differences in cerebellar V_Ts between baseline and blocking studies, with a good agreement between cerebellar V_Ts and Lassen plot–derived V_{ND}s. Taken together, the data support the use of the cerebellum as a reference region for estimation of BP_{ND}s.

The ^{18}F-MNI698 test–retest variability determined here compares favorably with the previously reported test–retest variability of ^{11}C-SB207145 (*18*), and it was lowest when noninvasive methods were used for data quantification, which could be attributed to blood measurement errors leading to an increase of test–retest variability when using invasive methods.

The measured upper mass dose limits for ^{18}F-MNI698 were 13.1–27.6 μg per 70 kg of body weight. Knowing a radiotracer upper mass dose limits is of key importance to establish acceptable specific activity levels during radiotracer quality control procedures and to ensure that the PET data acquired is not affected by any mass dose effects. Although it is unlikely that the no-observable-effect level would be breached at injected doses below the mass dose upper limit, evaluating the no-observable-effect level before future human studies might be required.

The radiotracer binding was blocked in a dose-dependent manner by SB204070 (drug dose resulting in 50% receptor occupancy was 1.5 μg/kg), confirming the selectivity of ^{18}F-MNI698-specific signal for the 5HT4R. Data also showed that, despite the negative bias of BP_{ND}s determined with noninvasive methods, compared with invasive methods of analysis, the occupancy measured by noninvasive methods correlated strongly with the occupancy measured with invasive methods and this relationship was close to the line of identity.

Studies presented here were acquired under anesthesia with isoflurane, a commonly used anesthetic for in vivo imaging. Serotonin, like other biologic molecules, is involved in multiple physiologic systems of relevance during anesthesia, and evidence has shown that anesthesia can play a potential role in radiotracer uptake and binding (*28,29*). Thus, it is possible that the use of anesthesia could have a secondary effect on ^{18}F-MNI698 uptake and binding. Nonetheless, despite its drawbacks (consequence of direct effects on physiologic functions), properly monitored anesthesia can often provide suitable conditions for in vivo imaging of the living brain of laboratory animals.

For the experiments reported here, ^{18}F-MNI698 was obtained with approximately 3% decay-corrected radiochemical yield. Improvement of this yield is desirable, especially for future multicenter human studies. Thus, work to optimize ^{18}F-MNI698 radiochemical yield is under way, now that we have established that ^{18}F-MNI698 is a promising radiotracer for imaging of 5HT4R in brain.

CONCLUSION

^{18}F-MNI698 displayed a good brain penetration in monkeys and its distribution in the brain was consistent with known 5HT4R densities. High BP_{ND}s were measured in target regions and a good test–retest variability was determined. Data indicate that the cerebellum can be used as a reference region for data quantification, although BP_{ND}s measured with noninvasive methods, compared with invasive methods, are biased, especially in regions with high 5HT4R density. The ^{18}F-MNI698 mass dose upper limit (occupancy $< 5\%$) was found to be 13.1 μg per 70 kg of body weight. Finally, ^{18}F-MNI698 binding in target regions was blocked by the selective 5HT4R antagonist SB204070 in a dose-dependent manner, confirming the radiotracer-specific signal for the 5HT4R. Human studies are warranted based on these study results.

TABLE 4
Summary of Injected Mass Doses Normalized to 70 Kilograms of Body Weight and Corresponding Estimates of ID_{50}, D_{10}, and D_5

Rhesus monkey identification no.	Mass dose (μg)		Occupancy plots		Mass dose limits (μg)		
	D_{Low}	D_{High}	α	R^2	ID_{50}	D_5	D_{10}
1	2.88	128.26	0.63	0.99	208.33	10.96	23.15
2	7.39	110.05	0.72	0.99	288.24	15.17	32.03
Mean ± SD	5.13 ± 3.19	119.15 ± 12.88	0.68 ± 0.06		248.29 ± 56.50	13.07 ± 2.98	27.59 ± 6.28

D_{Low} = low mass dose; D_{High} = high mass dose.

DISCLOSURE

The costs of publication of this article were defrayed in part by the payment of page charges. Therefore, and solely to indicate this fact, this article is hereby marked "advertisement" in accordance with 18 USC section 1734. No potential conflict of interest relevant to this article was reported.

ACKNOWLEDGMENTS

We thank Yun Zhang for assistance with metabolite analysis and Amy Amenta for technical assistance with studies preparation and logistics.

REFERENCES

1. Bockaert J, Claeysen S, Compan V, Dumuis A. 5-HT_4 receptors: history, molecular pharmacology and brain functions. *Neuropharmacology.* 2008;55:922–931.
2. Bockaert J, Claeysen S, Compan V, Dumuis A. 5-HT_4 receptors, a place in the sun: act two. *Curr Opin Pharmacol.* 2011;11:87–93.
3. Hegde SS, Eglen RM. Peripheral 5-HT_4 receptors. *FASEB J.* 1996;10:1398–1407.
4. Varnäs K, Halldin C, Pike VW, Hall H. Distribution of 5-HT_4 receptors in the postmortem human brain: an autoradiographic study using [^{125}I]SB 207710. *Eur Neuropsychopharmacol.* 2003;13:228–234.
5. Vilaró MT, Cortés R, Gerald C, Branchek TA, Palacios JM, Mengod G. Localization of 5-HT_4 receptor mRNA in rat brain by in situ hybridization histochemistry. *Brain Res Mol Brain Res.* 1996;43:356–360.
6. Ansanay H, Sebben M, Bockaert J, Dumuis A. Pharmacological comparison between [^{3}H]GR 113808 binding sites and functional 5-HT_4 receptors in neurons. *Eur J Pharmacol.* 1996;298:165–174.
7. Reynolds GP, Mason SL, Meldrum A, et al. 5-hydroxytryptamine $(5\text{-HT})_4$ receptors in *post mortem* human brain tissue: distribution, pharmacology and effects of neurodegenerative diseases. *Br J Pharmacol.* 1995;114:993–998.
8. Lucas G, Rymar VV, Du J, et al. Serotonin 4 (5-HT_4) receptor agonists are putative antidepressants with a rapid onset of action. *Neuron.* 2007;55:712–725.
9. Tamburella A, Micale V, Navarria A, Drago F. Antidepressant properties of the 5-HT_4 receptor partial agonist, SL65.0155: behavioral and neurochemical studies in rats. *Prog Neuropsychopharmacol Biol Psychiatry.* 2009;33:1205–1210.
10. Vidal R, Valdizan E, Vilaró MT, Pazos A, Castro E. Reduced signal transduction by 5-HT_4 receptors after long-term venlafaxine treatment in rats. *Br J Pharmacol.* 2010;161:695–706.
11. Li J, Wang Y, Zhou R, et al. Association of attention-deficit/hyperactivity disorder with serotonin 4 receptor gene polymorphisms in Han Chinese subjects. *Neurosci Lett.* 2006;401:6–9.
12. Jean A, Laurent L, Bockaert J, et al. The nucleus accumbens 5-HTR_4-CART pathway ties anorexia to hyperactivity. *Transl Psychiatry.* 2012;2:e203.
13. Haahr ME, Rasmussen PM, Madsen K, et al. Obesity is associated with high serotonin 4 receptor availability in the brain reward circuitry. *Neuroimage.* 2012;61:884–888.
14. Shen F, Smith JAM, Chang R, et al. 5-HT4 receptor agonist mediated enhancement of cognitive function in vivo and amyloid precursor protein processing in vitro: a pharmacodynamic and pharmacokinetic assessment. *Neuropharmacology.* 2011;61:69–79.
15. Tesseur I, Pimenova AA, Lo AC, et al. Chronic 5-HT_4 receptor activation decreases Aβ production and deposition in hAPP/PS1 mice. *Neurobiol Aging.* 2013;34:1779–1789.
16. Gee AD, Martarello L, Passchier J, et al. Synthesis and evaluation of [^{11}C]SB207145 as the first *in vivo* serotonin 5-HT_4 receptor radioligand for PET imaging in man. *Curr Radiopharm.* 2008;1:110–114.
17. Kornum BR, Lind NM, Gillings N, Marner L, Andersen F, Knudsen GM. Evaluation of the novel 5-HT_4 receptor PET ligand [^{11}C]SB207145 in the Göttingen minipig. *J Cereb Blood Flow Metab.* 2009;29:186–196.
18. Marner L, Gillings N, Comley RA, et al. Kinetic modeling of ^{11}C-SB207145 binding to 5-HT_4 receptors in the human brain in vivo. *J Nucl Med.* 2009;50:900–908.
19. Pike VW, Halldin C, Nobuhara K, et al. Radioiodinated SB 207710 as a radioligand in vivo: imaging of brain 5-HT_4 receptors with SPET. *Eur J Nucl Med Mol Imaging.* 2003;30:1520–1528.
20. Caillé F, Morley TJ, Tavares AAS, et al. Synthesis and biological evaluation of positron emission tomography radiotracers targeting serotonin 4 receptors in brain: [^{18}F]MNI-698 and [^{18}F]MNI-699. *Bioorg Med Chem Lett.* 2013;23:6243–6247.
21. Innis RB, Cunningham V, Delforge J, et al. Consensus nomenclature for *in vivo* imaging of reversibly binding radioligands. *J Cereb Blood Flow Metab.* 2007;27:1533–1539.
22. Logan J. Graphical analysis of PET data applied to reversible and irreversible tracers. *Nucl Med Biol.* 2000;27:661–670.
23. Lammertsma AA, Hume SP. Simplified reference tissue model for PET receptor studies. *Neuroimage.* 1996;4:153–158.
24. Logan J, Fowler JS, Volkow ND, Wang G-J, Ding Y-S, Alexoff DL. Distribution volume ratios without blood sampling from graphical analysis of PET data. *J Cereb Blood Flow Metab.* 1996;16:834–840.
25. Madsen K, Marner L, Haahr M, Gillings N, Knudsen GM. Mass dose effects and in vivo affinity in brain PET receptor studies: a study of cerebral 5-HT_4 receptor binding with [^{11}C]SB207145. *Nucl Med Biol.* 2011;38:1085–1091.
26. Cunningham VJ, Rabiner EA, Slifstein M, Laruelle M, Gunn R. Measuring drug occupancy in the absence of a reference region: the Lassen plot re-visited. *J Cereb Blood Flow Metab.* 2010;30:46–50.
27. Marner L, Gillings N, Madsen K, et al. Brain imaging of serotonin 4 receptors in humans with [^{11}C]SB207145-PET. *Neuroimage.* 2010;50:855–861.
28. Hildebrandt IJ, Su H, Weber WA. Anesthesia and other considerations for in vivo imaging of small animals. *ILAR J.* 2008;49:17–26.
29. Alstrup AKO, Smith DF. Anaesthesia for positron emission tomography scanning of animal brains. *Lab Anim.* 2013;47:12–18.